

Laser-induced fluorescence measurements in an inductively coupled plasma reactor

Brett Jacobs,^{a)} Walter Gekelman, and Pat Pribyl

Department of Physics, University of California, Los Angeles, California 90095, USA

Michael Barnes

Intevac Corporation, Santa Clara, California 95054, USA

Michael Kilgore

Novellus Corporation, San Jose, California 95134, USA

(Received 3 July 2007; accepted 2 October 2007; published online 19 October 2007)

The authors report on laser-induced fluorescence (LIF) measurements of ion velocity distribution functions made in an inductively coupled plasma reactor with a pulsed plasma source. Vertical and radial velocities have been measured at thousands of spatial locations within a plane, and the LIF data have been calibrated to a 96 GHz microwave interferometer. The ions are observed to approach the Bohm velocity and the inferred electric potential within the presheath agrees well with theory. A two-dimensional flow pattern of the ion velocity above the substrate is presented.

© 2007 American Institute of Physics. [DOI: 10.1063/1.2801393]

In plasma processing of semiconductors, control of the energy and velocity of ions incident on the substrate is critical. Etching and gap fill applications are especially sensitive to the collimation of the ion flux. Measurement of these parameters in the plasma sheath above the substrate by an *in situ* probe is impractical because of the sheath surrounding the probe itself. Laser-induced fluorescence (LIF) is a non-invasive optical technique for measuring the ion velocity distribution function, $f(\mathbf{v})$, in a plasma¹ with good spatial² and temporal³ resolutions and has been used to probe the sheath^{4,5} and presheath⁶⁻⁸ regions. Zimmerman *et al.* have used a two-dimensional (2D) tomographic, single point LIF technique in an ion beam source.⁹ Other optical techniques such as LIF dip¹⁰ and Fabry-Pérot interferometry¹¹ have also been used to investigate ion dynamics in rf plasmas.

This letter will report on 2D ion velocity distribution functions measured with LIF simultaneously at thousands of spatial points in a plane above the wafer of a commercial plasma processing machine. In LIF, a narrow bandwidth laser stimulates a resonant electronic transition of the ion species from a metastable state (1 μs lifetime) to an excited state. This excited state is short lived (3 ns lifetime) and spontaneously decays to a third state with the emission of a fluorescence photon at a different wavelength.

Ions with motion along the direction of the laser propagation will have their resonances Doppler shifted. The formula

$$2\pi\Delta\nu = 2\pi(v_L - v_0) = \mathbf{v} \cdot \mathbf{k}_L = v_{\parallel}k_L \quad (1)$$

gives the resonance condition, with laser frequency v_L , ion resonance frequency v_0 , ion velocity \mathbf{v} , and laser wavenumber \mathbf{k}_L .

A laser tuned to a frequency v_L is actually composed of a spectrum of frequencies centered about v_L . Although the precise details of the laser spectrum depend on various conditions within the laser cavity, a Gaussian frequency distribution is an excellent approximation. Assuming a thermal

distribution of ions, the one-dimensional ion $f_i(v_{\parallel})$ will also be Gaussian, with a full width at half maximum of δv_i in frequency space. The LIF distribution is obtained by scanning the laser central frequency v_L over the ion resonance. The resulting LIF signal $f(v_L)$ will also be a Gaussian, which is proportional to the convolution of $f_L(v)$ with $f_i(v)$. For $T_i=1$ eV and $\delta v_L=1.091$ GHz, the measured argon LIF distribution will have a temperature of 1.033 eV and closely resemble the true ion distribution function.

The plasma processing tool used in this experiment was a 200 mm high-density plasma chemical vapor deposition speed tool from Novellus. The chamber was cylindrical ($r=20$ cm, $h=30$ cm) with a pulsed, inductively coupled plasma source (400 Hz repetition rate at 400 kHz). The instantaneous plasma source power was 4 kW, with an argon fill pressure of 4.5 mTorr.

This LIF diagnostic used a pulsed, tunable dye laser which was pumped by a 10 ns Nd:YAG (yttrium aluminum garnet) laser. The laser light was shaped into a thin (0.6 mm thick \times 50 mm wide) sheet by cylindrical optics. Two identical sets of sheet optics were mounted on the chamber to measure either the vertical or radial components of $f(\mathbf{v})$ in an overlapping plane.

The laser was tuned near a resonance at 611.492 nm to excite ions from the metastable $3D' \ ^2G_{9/2}$ state to $4P' \ ^2F_{7/2}$ which then decayed to $4S' \ ^2D_{5/2}$ with the emission of a fluorescence photon at 460.957 nm (wavelengths given in air).

A fast, intensified charge coupled device (CCD) camera recorded the fluorescence from the ions as the laser's wavelength was tuned across the resonance line (see Fig. 1). A narrow ($\Delta\lambda=1$ nm) bandpass interference filter centered at 461 nm blocked more than 99% of the background and scattered laser light from entering the camera. Each pixel in the 320×256 camera images corresponds to an area of $500 \times 500 \mu\text{m}^2$ within the imaged plane, which sets the spatial resolution of the diagnostic.

The laser pulse was phase locked to the rf source waveform. Temporal resolution of the diagnostic is limited by the 10 ns time duration of the laser pulse.

^{a)}Electronic mail: bjacobs@physics.ucla.edu

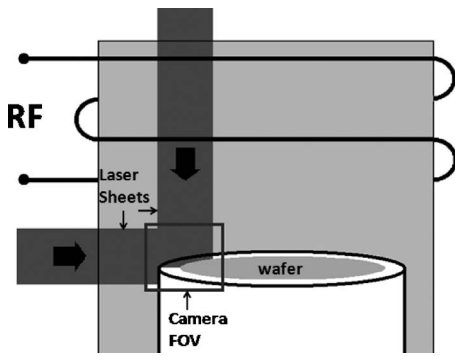


FIG. 1. Chamber diagram showing vertical and radial laser sheets and the CCD camera's field of view.

The high powers of pulsed lasers can easily distort the shape of the measured $f(v)$ by an effect called saturation (or power) broadening.¹² When the laser intensity is great enough to excite nearly all of the metastable ions with velocities lying within the bandwidth of the laser, the wings of the laser's frequency distribution become important. The relatively small amount of laser radiation outside the laser's bandwidth will normally excite only a negligible amount of ions. At very high laser power, the fluorescence signal from these ions will be comparable to that from the ions within the nominal velocity window. This will effectively increase the laser's bandwidth and smear out the shape of the measured curve. Using the technique outlined by Goeckner and Gorree, an optimum laser power was found which avoided power broadening while still achieving a good signal to noise ratio.¹²

Line-integrated electron density was measured in the bulk plasma with a standard 96 GHz heterodyne microwave interferometer. The interferometer measurements had an accuracy of $\pm 2 \times 10^{10} \text{ cm}^{-3}$ and were used to calibrate the LIF measurements. A typical vertical component of $f(v)$ is shown in Fig. 2(a). These data were taken at a point 20 mm above the wafer surface, in the bulk plasma. The measured $f(v_z)$ is a good, but imperfect fit to a 0.8 eV Gaussian distribution, indicating that the ions are not purely thermal. The signal to noise ratio of the diagnostic is about 20:1.

The width of the presheath is given by the ion mean free path (collisions with neutrals dominate in this plasma, with

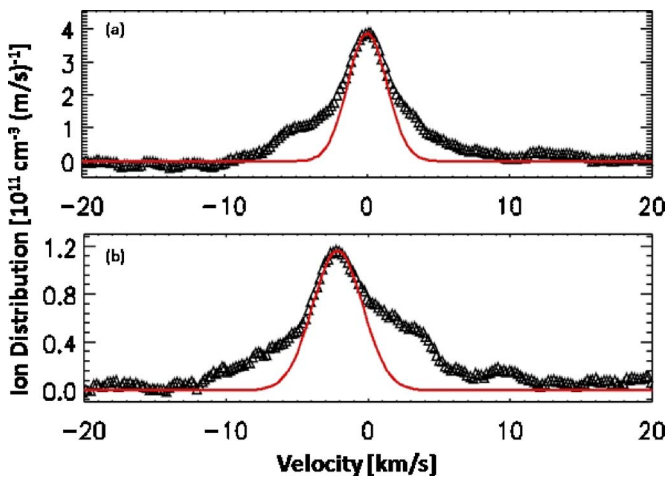


FIG. 2. (Color online) (a) $f(v_z)$ at a point in the bulk plasma. The solid curve is a fit to a nondrifting 0.8 eV Gaussian. (b) $f(v_z)$ at a point in the presheath. The solid curve is a fit to a 1.3 eV Gaussian drifting downward at 2.1 km/s.

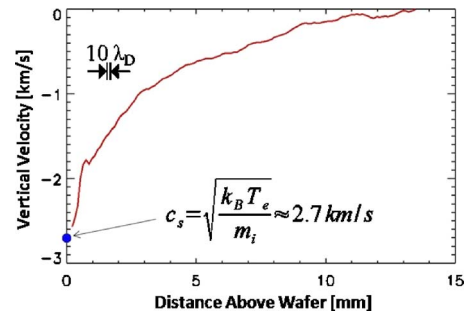


FIG. 3. (Color online) Vertical ion drift velocities in the presheath.

$\lambda_{\text{mfp}} = 10 \text{ mm}$) and is typically much larger than the sheath region, which is about $10\lambda_D$ or $100 \mu\text{m}$. Quasineutrality holds in the presheath but there is a small electric field accelerating ions from the bulk plasma into the sheath. Bohm has shown that ions must reach the ion sound speed by the time they reach the sheath/presheath boundary.^{6,7} An $f(v_z)$ in the presheath region, 2 mm above the wafer surface is shown in Fig. 2(b).

There is clearly a population drifting downward toward the wafer with approximately the same temperature as the bulk plasma. A smaller, nondrifting population of ions is also visible in the $f(v)$ —this may be due to neutrals which are ionized by collisions within the presheath. These recently ionized particles have not had time to be accelerated by the presheath potential, and therefore have velocities centered about $v_z = 0$.

Figure 3 shows a plot of vertical drift velocity versus height above the wafer. The ion drift velocity is taken to be the peak of $f(v)$ in velocity space.

Ions more than 10 mm from the wafer have $f(v_z)$ centered about zero, indicating that they are in the bulk of the plasma. Downward ion drifts develop closer to the wafer. The width of the drifting region (about 12 mm) corresponds to the size of the presheath and agrees with the ion mean free path of 10 mm.

The Bohm criterion predicts that ions will reach the sound speed of the system as they travel from the presheath into the sheath. For $T_e = 3 \text{ eV}$, $c_s = 2.6 \text{ km/s}$, which is nearly reached by ions just above the wafer. The camera's resolution is on the order of the sheath thickness, and therefore, $f(v)$ could not be measured inside the sheath with the current setup. Assuming that the presheath electric potentials are solely responsible for the ion drifts, the potential profile can be obtained from energy conservation (see Fig. 4).

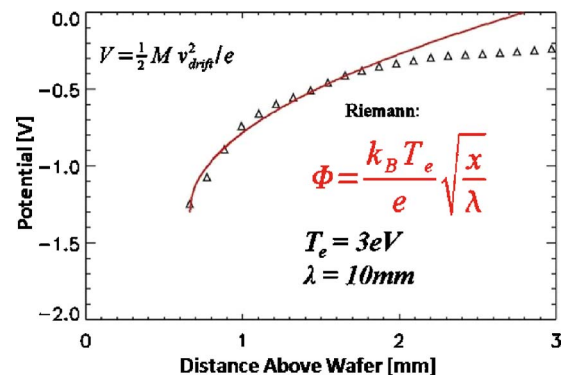


FIG. 4. (Color online) Electric potential in presheath, solid curve is fit to theory.

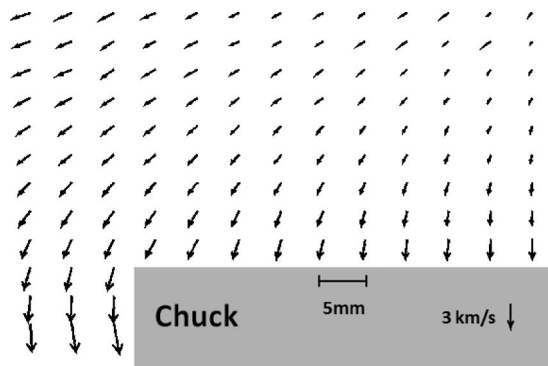


FIG. 5. Vector map of ion drift velocities. The wafer is just above the electrostatic chuck, shown in gray. Vectors are shown every ten grid points and should be compared to the reference vector inside the chuck with length of 3 km/s.

Riemann has predicted that the potential in the presheath region just above the sheath boundary will vary as the square root of the position.¹³ This theory is a good fit to the measured potentials in the lower 1–2 mm of the presheath.

By combining the vertical and radial drifts at many points in the plane, 2D maps of ion motion can be obtained, as shown in Fig. 5. Measurements at different phases of the rf source waveform yield nearly identical $f(\mathbf{v})$. This is expected, as the source fields only penetrate a few centimeters into the plasma.

In conclusion, this planar laser-induced fluorescence diagnostic has measured ion velocity distribution functions with unprecedented resolution and completeness. The obtained ion drift velocities and inferred electric potentials agree well with theory within the presheath region. This diagnostic is especially well suited for examining the uniformity of $f(\mathbf{v})$, since thousands of spatial points across the wafer are probed simultaneously.

Applying a rf bias voltage to the wafer will change $f(\mathbf{v})$ considerably. The maximum vertical drift velocity will be much higher, and the sheath and presheath thicknesses will both increase. Ion collimation should be improved if the radial drifts remain constant and the substrate bias draws ions straight down. The next measurements will include rf bias.

Simulations and theory predict that in certain conditions, rf bias can create ion $f(\mathbf{v})$'s with two peaks at different energies.¹⁴ The two peaks are a result of the spatial and temporal variations of the rf sheath. Detailed investigations of the dynamics within rf sheaths will provide direction on improving simulation models.

Future measurements will be conducted in gas mixtures of argon and oxygen. Oxygen mimics the electronegative properties of many gases used in etch and deposition processes, providing a more realistic plasma environment.

This research was supported by the State of California and Novellus Corporation under the California MICRO program under Grant No. 05-080.

- ¹R. A. Stern and J. A. Johnson III, Phys. Rev. Lett. **34**, 1548 (1975).
- ²G. A. Hebner, J. Appl. Phys. **80**, 2624 (1996).
- ³I. A. Biloiu, X. Sun, and E. Scime, Rev. Sci. Instrum. **77**, 10F301 (2006).
- ⁴M. J. Goeckner, J. Goree, and T. E. Sheridan, Phys. Fluids B **4**, 1663 (1992).
- ⁵B. K. Woodcock, J. R. Busby, T. G. M. Freearge, and G. Hancock, J. Appl. Phys. **81**, 5945 (1996).
- ⁶G. D. Severn, X. Wang, E. Ko, and N. Hershkowitz, Phys. Rev. Lett. **90**, 145001 (2003).
- ⁷X. Wang and N. Hershkowitz, Phys. Plasmas **13**, 053503 (2006).
- ⁸L. Oksuz, M. Atta Khedr, and N. Hershkowitz, Phys. Plasmas **8**, 5 (2001).
- ⁹D. C. Zimmerman, R. McWilliams, and D. A. Edrich, Plasma Sources Sci. Technol. **14**, 581 (2005).
- ¹⁰E. V. Barnat and G. A. Hebner, Appl. Phys. Lett. **69**, 3393 (2004).
- ¹¹J. A. O'Neill, M. S. Barnes, and J. H. Keller, J. Appl. Phys. **73**, 1621 (1993).
- ¹²M. J. Goeckner and J. Goree, J. Vac. Sci. Technol. A **7**, 977 (1988).
- ¹³K.-U. Riemann, Phys. Plasmas **4**, 4158 (1997).
- ¹⁴D. Vender and R. W. Boswell, IEEE Trans. Plasma Sci. **18**, 4 (1990).